

Herschel observations of ortho- and para-oxidaniumyl (H_2O^+) in spiral arm clouds toward Sgr B2(M) \star

P. Schilke,^{1,2} C. Comito,² H. S. P. Müller,¹ E. A. Bergin,³ E. Herbst,¹⁴ D. C. Lis,⁴ D. A. Neufeld,²⁰ T. G. Phillips,⁴ T. A. Bell,⁴ G.A. Blake,⁵ S. Cabrit,²⁴ E. Caux,^{6,7} C. Ceccarelli,⁸ J. Cernicharo,⁹ N. R. Crockett,³ F. Daniel,^{9,10} M.-L. Dubernet,^{11,12} M. Emprechtinger,⁴ P. Encrenaz,¹⁰ M. Gerin,¹⁰ T. F. Giesen,¹ J. R. Goicoechea,⁹ P. F. Goldsmith,¹³ H. Gupta,¹³ C. Joblin,^{6,7} D. Johnstone,¹⁵ W. D. Langer,¹³ W. B. Latter,¹⁶ S. D. Lord,¹⁶ S. Maret,⁸ P. G. Martin,¹⁷ G. J. Melnick,¹⁸ K. M. Menten,² P. Morris,¹⁶ J. A. Murphy,¹⁹ V. Ossenkopf,^{12,21} L. Pagani,²⁴ J. C. Pearson,¹³ M. Pérault,¹⁰ R. Plume,²² S.-L. Qin,¹³ M. Salez,²⁴ S. Schlemmer,¹ J. Stutzki,¹ N. Trappe,¹⁹ F. F. S. van der Tak,²¹ C. Vastel,^{6,7} S. Wang,³ H. W. Yorke,¹³ S. Yu,¹³ N. Erickson,²⁵ F.W. Maiwald,¹³ J. Kooi,⁴ A. Karpov,⁴ J. Zmuidzinas,⁴ A. Boogert,⁴ R. Schieder,¹ and P. Zaal²¹

(Affiliations can be found after the references)

Preprint online version: September 22, 2018

ABSTRACT

H_2O^+ has been observed in its *ortho*- and *para*- states toward the massive star forming core Sgr B2(M), located close to the Galactic center. The observations show absorption in all spiral arm clouds between the Sun and Sgr B2. The average o/p ratio of H_2O^+ in most velocity intervals is 4.8, which corresponds to a nuclear spin temperature of 21 K. The relationship of this spin temperature to the formation temperature and current physical temperature of the gas hosting H_2O^+ is discussed, but no firm conclusion is reached. In the velocity interval 0-60 km s⁻¹, an *ortho/para* ratio of below unity is found, but if this is due to an artifact of contamination by other species or real is not clear.

Key words. ISM: abundances — ISM: molecules

1. Introduction

Simple di- and triatomic molecules and ions are fundamental constituents of interstellar chemistry which eventually leads to the formation of complex molecules. Many of these species have ground state transitions at submillimeter- and THz wavelengths, and are therefore either difficult or not at all observable from the ground, yet they constitute the building blocks of chemistry, and are therefore fundamental to its understanding in various environments. Among those are spiral arm clouds, located in the plane of the Galactic disk, where the line-of-sight toward a strong continuum source passes through by chance. This setup allows sensitive absorption measurements, and the clouds have been observed by this method against the Sgr B2, W31c, W49, W51 and CasA millimeter continuum sources using molecular species such as CO, HCN, HCO⁺, CS, CN, SO, and c-C₃H₂ etc (e.g. Greaves & Williams, 1994; Tieftrunk et al., 1994; Greaves & Nyman, 1996; Menten et al., 2010; Gerin et al., 2010; Ossenkopf et al., 2010). The results demonstrate that spiral arm clouds have low gas density and low excitation temperatures, and represent diffuse and translucent clouds.

One of the best sources for these absorption studies is Sgr B2, located close to the Galactic center, ~ 100 pc from Sgr A^{*} in projection, and one of the strongest submillimeter sources in the Galaxy (e.g. Pierce-Price et al., 2000). The dense cores Sgr B2(N) and Sgr B2(M) within the cloud are at different evo-

lutionary stages, and constitute well-studied massive star forming regions in our Galaxy. The flux ratio of the continuum between Sgr B2(M) and Sgr B2(N) is less than unity at 1 mm and rises at shorter wavelengths so that Sgr B2(M) dominates above ~ 500 GHz (Goldsmith et al., 1990; Lis & Goldsmith, 1991). Sgr B2(M) also shows fewer molecular emission lines than Sgr B2(N) (Nummelin et al., 1998), hence less confusion and therefore is better suited for absorption studies. The line-of-sight toward the Sgr B2(M) continuum will pass almost all the way to the center of our Galaxy, providing a more complete census in studying physical and chemical conditions towards the Galactic center clouds and all spiral arm clouds simultaneously. HIFI, the Heterodyne Instrument for the Far-Infrared (de Graauw et al., 2010) on board the *Herschel* Space Observatory (Pilbratt et al., 2010) is an ideal instrument for making these observations.

2. Observations

Full spectral scans of HIFI bands 1a, 1b, and 4b towards Sgr B2(M) ($\alpha_{J2000} = 17^{\text{h}}47^{\text{m}}20.35^{\text{s}}$ and $\delta_{J2000} = -28^{\circ}23'03.0''$) have been carried out respectively on **March 1, 2, and 5 2010**, providing coverage of the frequency range 479 through 637 GHz and 1051 through 1121 GHz.

HIFI Spectral Scans are carried out in Dual Beam Switch (DBS) mode, where the DBS reference beams lie approximately 3' apart. The wide band spectrometer (WBS) is used as a back-end, providing a spectral resolution of 1.1 MHz over a 4-GHz-wide Intermediate Frequency (IF) band. A HIFI Spectral Scan consists of a number of double-sideband (DSB) spectra, tuned at different Local Oscillator (LO) frequencies, where the spacing between one LO setting and the next is determined by the

\star *Herschel* is an ESA space observatory with science instruments provided by European-led Principal Investigator consortia and with important participation from NASA.

“redundancy” chosen by the observer Comito & Schilke (2002). The molecular spectrum of Sgr B2(M) in band 1a and 4b has been scanned with a redundancy of 4, that of band 1b with a redundancy of 8, which means that every frequency has been observed respectively 4 and 8 times in each sideband. Multiple observations of the same frequency at different LO tunings are necessary to separate the lower-sideband (LSB) from the upper-sideband (USB) spectrum.

The data have been calibrated through the standard pipeline released with version 2.9 of HIPE Ott et al. (2010), and subsequently exported to CLASS¹ using the HiClass task within HIPE. Deconvolution of the DSB data into single-sideband (SSB) format has been performed on CLASS. All the HIFI data presented here, spectral features *and* continuum emission, are deconvolved SSB spectra. Although both horizontal (H) and vertical (V) polarizations have been obtained, we will show only H-polarization spectra. The intensity scale is main-beam temperature, and results from applying a beam efficiency correction of 0.69 for band 1a, 0.68 for band 1b, and 0.669 for band 4b (Roelfsema P., Helmich F.P., Teyssier, D. et al., 2010).

3. Spectroscopy of H₂O⁺

Removal of an electron from oxidane, H₂O, also known as water, yields oxidaniumyl, H₂O⁺. Its bond lengths and bond angle are slightly larger than those of H₂O, see e.g. Strahan et al. (1986). Quantum-chemical calculations (Weis et al., 1989) yielded a ground state dipole moment of ~ 2.4 D, considerably larger than in H₂O. The transitions are of *b*-type, meaning $\Delta K_a \equiv \Delta K \equiv 1 \pmod{2}$. The electronic ground state changes from ¹A₁ in the neutral to ²B₁ in the cation which leads to a reversal of the *ortho* and *para* levels with respect to water. $K_a + K_c$ is even and odd for *ortho*- and *para*-H₂O⁺, respectively. The *para* levels do not show any hyperfine splitting while the *ortho* levels are split into three because of the ¹H hyperfine structure. The strong lines have $\Delta F = \Delta J = \Delta N$, i.e. they do not involve a spin-flip. At low quantum numbers spin-flipping transitions have appreciable intensity.

Further details of the spectroscopy of H₂O⁺ are discussed in the Appendix. Table A.1 provides calculated rest frequencies for the two rotational transitions discussed in the present investigation. Fig. A.1 show the lowest energy levels of H₂O⁺ with allowed transitions.

4. Results

Determining the opacities and thus column densities of absorption lines is traditionally done using the line-to-continuum ratio. In the present case, this is not straightforward, because the *ortho*-H₂O⁺-line has hyperfine structure with closeby components (Fig. 1), which distorts the simple correspondence of line-to-continuum ratio with column density at a given velocity, and also because the line background of the Sgr B2(M) core cannot necessarily be neglected. We therefore fitted the lines using the XCLASS² program, which performs an LTE fit using the molecular data discussed in Sect. 3, using the automated fit-

ting routine provided by MAGIX³. For all velocity components, an excitation temperature of 2.7 K was assumed. For molecules that react strongly with H₂ (see the discussion in Black, 1998; Stauber & Bruderer, 2009), the collisional processes in diffuse gas are unimportant relative to radiative excitation in controlling the excitation temperatures of observed transitions of species with high dipole moments such as H₂O⁺, since inelastic collisions with H, H₂ and electrons compete with reactive collisions. The excitation temperature employed here may still not be entirely correct, since particularly at 1115 GHz the general FIR background of the Galaxy contributes to a radiation temperature of 4.8 K even in the vicinity of the Sun, and for the spiral arm clouds one expects similar or slightly higher values (Wright et al., 1991; Paladini et al., 2007). Our analysis is not affected however if the excitation temperature is dominated by this radiation field, and stays significantly smaller compared with the upper level energies for the *para*- and *ortho*-H₂O⁺ ground state lines $h\nu/k = 29$ and 54 K, respectively, which is a well justified assumption. The maximum opacities of the *ortho*-H₂O⁺ line are about 2, so the lines are only moderately opaque.

For *para*-H₂O⁺, only the 607 GHz line was used to perform the fit, since this is the strongest and least contaminated *para*-line, but it can be seen from Fig. 2 that predictions from this reproduce the other *para* lines rather well. To predict contamination, we used the fit of all species in Sgr B2(M) (Qin et al, in prep) as background. This is a preliminary version of the fit, and we cannot exclude the existence of additional contamination by unknown lines. Thus we estimate the error of the fit due to uncertainties of this nature very conservatively to be 20%, but in the presence of strong unknown lines it could be larger at certain frequencies. This is particularly true for the possible D₂O contamination of the *para*-H₂O⁺-line at 607 GHz. The relatively small variation of the *ortho/para* ratio in the absorption cloud range (see below) argues against contamination by a strong unknown line however. All *para*-H₂O⁺ components are optically thin. In the following, we make the assumption that the excitation of all upper levels can be approximated as LTE with an excitation temperature of 2.7 K, and that thus the *ortho*- and *para*-H₂O⁺ column densities can be measured by observations of the ground state. This assumption is reasonable for the spiral arm clouds, but most likely violated for the clouds associated with the Sgr B2(M) envelope (see below).

It appears that the absorption lines of different species toward Sgr B2(M) cannot be fitted with a unique set of physical components of fixed velocity and velocity width. This probably reflects the different origins of the species in atomic, low density molecular and high density molecular gas with a different velocity structure. A detailed study of the different distributions will have to await the complete data set of the survey. Apart from that, particularly in species which have hyperfine structure and are very abundant, that is in species which absorb at all velocities, the decomposition into basically Gaussian components would not necessarily be unique. The fit rather represents a deconvolution of the hyperfine pattern. We therefore prefer to present the results as depicted in Fig. 3, as column densities/velocity interval and ratio as a function of velocity, as a sum over the components. The component of the Sgr B2(M) envelope, which is located at 64 km s⁻¹, is most uncertain, because here the *para*-H₂O⁺ 607 GHz line is most contaminated, and there the assumption of uniformly low excitation temperature for all levels is most likely to be violated, since this is warm and dense gas with a strong FIR field which may dominate the excitation.

¹ Continuum and Line Analysis Single-dish Software, distributed with the GILDAS software, see <http://www.iram.fr/IRAMFR/GILDAS>.

² We made use of the myXCLASS program (<https://www.astro.uni-koeln.de/projects/schilke/XCLASS>), which accesses the CDMS (Muller et al., 2001, 2005 <http://www.cdms.de>) and JPL Pickett et al., 1998 <http://spec.jpl.nasa.gov>) molecular data bases.

³ <https://www.astro.uni-koeln.de/projects/schilke/MAGIX>

Since H_2O^+ is expected to originate in mostly atomic gas at the edge of diffuse and translucent clouds, giving abundances relative to H_2 or H does not make sense, since it exists neither in purely atomic, nor in purely molecular gas. Menten et al. (2010) and Qin et al. (2010) give column densities of H_2 of typically a few times 10^{21} cm^{-2} and H column densities of typically 10^{20} cm^{-2} , so the average H_2O^+ abundance relative to the number of H nuclei is a few times 10^{-8} , but could be much higher locally. The *o/p* ratio was calculated using the column densities, and has a mean of 4.8 ± 0.5 for the spiral arm clouds, with little variation.

We calculated the nuclear spin temperature using

$$\frac{N(\textit{ortho}\text{-H}_2\text{O}^+)}{N(\textit{para}\text{-H}_2\text{O}^+)} = e^{\Delta E/kT_{\text{nuclear spin}}} \frac{Q_o}{Q_p} \quad (1)$$

with $\Delta E = 30.1 \text{ K}$, and $Q_{o,p}$ the partition function of *ortho*- H_2O^+ /*para*- H_2O^+ , respectively, given in the Appendix. The $Q_{o,p}$ include the rotational and nuclear spin part, and are referenced to a ground state energy of zero for both. Toward the spiral arm clouds, we find the mean nuclear spin temperature to be almost constant at $21 \pm 2 \text{ K}$. At this temperature range, the ratio of the partition functions is almost equal to one, and the temperature is mostly determined by the exponential factor.

In the velocity range from about 0 to 60 km s^{-1} , the *o/p* ratio drops to unity, much below the high-temperature limit of 3. This does not reflect any thermal equilibrium and cannot be explained by any known formation mechanism: at low temperatures, the *o/p* ratio is extremely high, since all the molecules are in their lowest (*ortho*) state, and at high temperatures the limit 3 is reached, given by the nuclear spin statistics. We can only speculate about the cause of this unexpected result: it could be either a measurement error, or a real effect. If it is a measurement error, either the *ortho*- H_2O^+ column density is underestimated, which could be caused by contamination from a strong emission line, or the *para*- H_2O^+ column density is overestimated, which could be due to contamination from another absorption line, or the excitation temperatures deviate from the 2.7 K we assumed in such a way to produce this effect. The latter could e.g. be produced by a bright FIR field at the location of the clouds. Taking the measured ratio at face value as the *o/p* ratio would imply that a process exists which produces *ortho*- H_2O^+ and *para*- H_2O^+ in equal amounts.

5. Discussion

Since there are no fast radiative transitions between *para*- H_2O^+ and *ortho*- H_2O^+ , the derived nuclear spin temperature is thought to be determined by chemical processes, either at formation or afterwards, since *para-ortho* transformation can only occur accompanied with a proton exchange reaction of one of the hydrogen nuclei. The only observed kinetic temperature estimates in these clouds are from Tieftrunk et al. (1994), based on NH_3 , and show values of $35 \pm 5 \text{ K}$ in the -100 km s^{-1} component (which is believed to originate in the Galactic center), below 20 K in the velocity range in the spiral arm clouds, while the -10 to 20 km s^{-1} component (also from the Galactic center) has temperatures exceeding 100 K (Gardner et al., 1988), and is most likely shock heated. There is no similarity to the more or less constant nuclear spin temperature of 21 K we derive for H_2O^+ formation in this range, which suggests that H_2O^+ and NH_3 trace very different gas components: H_2O^+ the warm outer photon dominated edge of clouds, NH_3 either the shielded and cold interior, or hot shocked gas, which also seems to be devoid of H_2O^+ . This picture of H_2O^+ formation at the edges of clouds, actually in regions where the gas is mostly atomic, is supported by

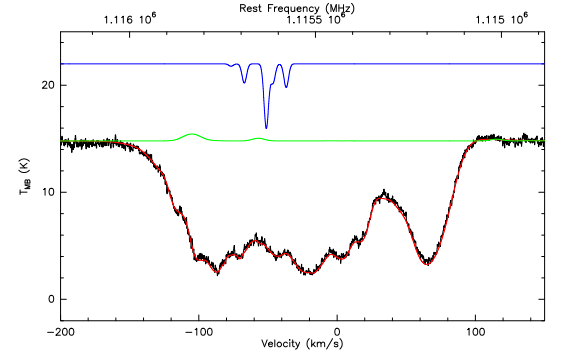


Fig. 1. *ortho*- H_2O^+ , as already shown in Ossenkopf et al. (2010). The data are shown in black, the fit in red, in blue the hfs pattern is depicted, and in green the predicted contamination by other molecules.

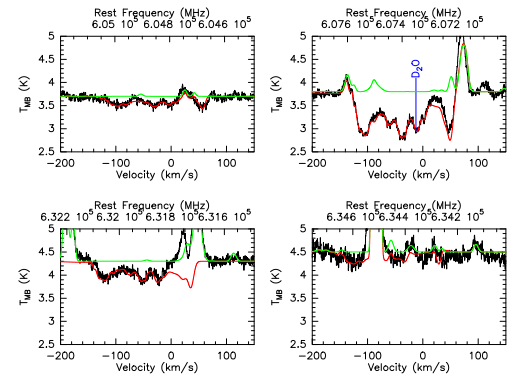


Fig. 2. *para*- H_2O^+ lines in Sgr B2, with the predicted contamination by other molecules in green, as in Fig. 1. The position of the D_2O ground state line is indicated.

Gerin et al. (2010) and Neufeld et al. (2010) based on studies of OH^+ and H_2O^+ with *Herschel*/HIFI. PDR models of diffuse clouds (Le Petit et al., 2006) predict temperatures of 50 to 100 K for the formation region of H_2O^+ in diffuse clouds ($A_V \approx 1\text{-}3$) with densities of about 10^2 and 10^3 cm^{-3} with radiation fields of 1-3 times ambient.

The relationship of nuclear spin temperature and formation or ambient temperature needs to be discussed in somewhat more detail (see Flower et al., 2006, for a discussion on this ratio for molecular hydrogen). H_2O^+ is a very reactive ion, and particularly it reacts exothermically with H_2 to form H_3O^+ , so the reaction *para*- $\text{H}_2\text{O}^+ + \text{H}_2 \rightarrow$ *ortho*- $\text{H}_2\text{O}^+ + \text{H}_2$, which would equilibrate the *o/p* ratio to the kinetic gas temperature, might not be relevant. If an equivalent reaction with atomic hydrogen (*para*- $\text{H}_2\text{O}^+ + \text{H} \rightarrow$ *ortho*- $\text{H}_2\text{O}^+ + \text{H}$) could happen, is unknown. If it does, it most likely will equilibrate to the current gas temperature, if not, the observed *o/p* ratio is the one established at formation. How this depends on the kinetic temperature at for-

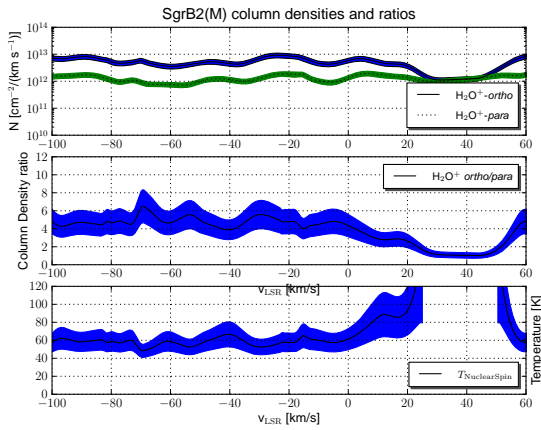


Fig. 3. Column density distribution of *ortho*-H₂O⁺ and *para*-H₂O⁺ (upper panel), o/p ratio (central panel) and $T_{\text{nuclearspin}}$ distribution (lower panel).

mation is not well understood. H₂O⁺ is produced by the highly exothermic reaction of OH⁺ with H₂, so the variables determining the H₂O⁺ o/p ratio are

1. the o/p ratio of H₂,
2. how much and in which way the excess energy of the exothermic reaction is available for o/p conversion of H₂O⁺,
3. the temperature of the gas at the time of formation, typically above 50–100 K based on PDR models.

The latter two processes would push the o/p ratio down toward 3:1, the high temperature value, which means toward a spin temperature higher than the 21 K we measure. The influence of the o/p ratio of H₂ is hard to assess: if the reaction proceeds by way of a collision complex, then the nuclear spin of H₂ will have an effect on the nuclear spin of product H₂O⁺, but not if the reaction proceeds through direct atom transfer. The measured o/p of H₂ in diffuse clouds is about unity (Savage et al., 1977; Rachford et al., 2009). Clearly, this is an interesting area of molecular physics that needs further study. From our observations, it seems that we see an excess of *ortho*-H₂O⁺ relative to what one would expect based on the formation temperature and available reaction energy in the spiral arm clouds and, if the measurement of an *ortho*-H₂O⁺/*para*-H₂O⁺ ratio in the 0 to 60 km s⁻¹ region is real, an excess of *para*-H₂O⁺ there. This velocity range nominally is assigned to the Sagittarius/Scutum arms (Vallée, 2008), outside of the Galactic center, where no exotic conditions are expected. However, this velocity range is also bracketed by gas local to Sgr B2 at 0 to 10 km s⁻¹ and around 60 km s⁻¹, so it could represent diffuse gas belonging to this complex, which could be the cause of unusual excitation or chemical conditions, e.g. due to shocks. In the lower velocity range overlapping with this (–10 to 20 km s⁻¹), Lis et al. (2010) also find water with an o/p ratio of 3, indicating high temperatures.

Lis et al. (2010) find an average spin temperature of 27 K for water toward the the spiral arms lines of sight. H₂O in these clouds is formed in the gas phase, through dissociative recombination of H₃O⁺, in a region where the gas is at about this temperature. The correspondence between physical temperature and spin temperature may be more easily traced by the more stable water molecule, although in general the contribution of grain surface chemistry for water complicates the issue (see discussion in Lis et al. 2010). From this study it is clear that by determining the *ortho/para*-ratio of H₂O⁺ (and, by proxy, from other simple

hydrides) one can learn a lot about the formation processes, but also that many fundamental physical and chemical processes are still not fully understood. We can look forward to the wealth of data HIFI will bring!

References

- Black, J. H. 1998, *Chemistry and Physics of Molecules and Grains in Space*. Faraday Discussions No. 109. The Faraday Division of the Royal Society of Chemistry, London, 1998., p.257, 109, 257
- Comito, C. & Schilke, P. 2002, *A&A*, 395, 357
- de Graauw, T., Helmich, F.P., Phillips, T.G. et al. 2010, *A&A*, 512
- Flower, D. R., Pineau Des Forêts, G., & Walmsley, C. M. 2006, *A&A*, 449, 621
- Gardner, F. F., Boes, F., & Winnewisser, G. 1988, *A&A*, 196, 207
- Gendriesch, R., Lewen, F., Winnewisser, G., & Müller, H. S. P. 2001, *J. Mol. Struct.*, 599, 293
- Gerin, M., De Luca, M., Black, J., et al. 2010, *ArXiv e-prints*
- Goldsmith, P. F., Lis, D. C., Hills, R., & Lasenby, J. 1990, *ApJ*, 350, 186
- Greaves, J. S. & Nyman, L. 1996, *A&A*, 305, 950
- Greaves, J. S. & Williams, P. G. 1994, *A&A*, 290, 259
- Le Petit, F., Nehmé, C., Le Bourlot, J., & Roueff, E. 2006, *ApJS*, 164, 506
- Lis, D., Phillips, T., Goldsmith, P., et al. 2010, *A&A*, this volume
- Lis, D. C. & Goldsmith, P. F. 1991, *ApJ*, 369, 157
- Margulès, L., Herbst, E., Ahrens, V., et al. 2002, *J. Mol. Spectrosc.*, 211, 211
- Menten, K., Wyrowski, F., Belloche, A., et al. 2010, *A&A*, submitted
- Müller, H. S. P., Schlöder, F., Stutzki, J., & Winnewisser, G. 2005, *Journal of Molecular Structure*, 742, 215227
- Müller, H. S. P., Thorwirth, S., Roth, D. A., & Winnewisser, G. 2001, *A&A*, 370, L49
- Mürtz, P., Zink, L. R., Evenson, K. M., & Brown, J. M. 1998, *J. Chem. Phys.*, 109, 9744
- Neufeld, D., Sonnentrucker, P., Goicoechea, J., et al. 2010, *A&A*, this volume
- Nummelin, A., Bergman, P., Hjalmarsen, A., et al. 1998, *ApJS*, 117, 427
- Ossenkopf, V., Müller, H. S. P., Lis, D. C., et al. 2010, *A&A*, 518
- Ott, S. 2010, in *ASP Conference Series, Astronomical Data Analysis Software and Systems XIX*, Y. Mizumoto, K.-I. Morita, and M. Ohishi, eds., in press
- Paladini, R., Montier, L., Giard, M., et al. 2007, *A&A*, 465, 839
- Pickett, H. M., Poynter, R. L., Cohen, E. A., et al. 1998, *Journal of Quantitative Spectroscopy and Radiative Transfer*, 60, 883890
- Pierce-Price, D., Richer, J. S., Greaves, J. S., et al. 2000, *ApJ*, 545, L121
- Pilbratt, G. L., Riedinger, J. R., Passvogel, T., et al. 2010, *A&A*, 518, L1
- Qin, S.-L., Schilke, P., Comito, C., et al. 2010, *A&A*, this volume
- Rachford, B. L., Snow, T. P., Destree, J. D., et al. 2009, *ApJS*, 180, 125
- Roelfsema, P. et al. 2010, *A&A*, this volume
- Savage, B. D., Bohlin, R. C., Drake, J. F., & Budich, W. 1977, *ApJ*, 216, 291
- Stäuber, P. & Bruderer, S. 2009, *A&A*, 505, 195
- Strahan, S. E., Mueller, R. P., & Saykally, R. J. 1986, *J. Chem. Phys.*, 85, 1252
- Tieftrunk, A., Pineau des Forêts, G., Schilke, P., & Walmsley, C. M. 1994, *A&A*, 289, 579
- Vallée, J. P. 2008, *AJ*, 135, 1301
- Weis, B., Carter, S., Rosmus, P., Werner, H., & Knowles, P. J. 1989, *J. Chem. Phys.*, 91, 2818
- Wright, E. L., Mather, J. C., Bennett, C. L., et al. 1991, *ApJ*, 381, 200
- Zheng, R., Li, S., Hou, S., Huang, G., & Duan, C. 2008, *Chin. Phys. B*, 17, 4485

¹ I. Physikalisches Institut, Universität zu Köln, Zùlpicher Str. 77, 50937 Köln, Germany

e-mail: schilke@ph1.uni-koeln.de

² Max-Planck-Institut für Radioastronomie, Auf dem Hügel 69, 53121 Bonn, Germany

³ Department of Astronomy, University of Michigan, 500 Church Street, Ann Arbor, MI 48109, USA

⁴ California Institute of Technology, Cahill Center for Astronomy and Astrophysics 301-17, Pasadena, CA 91125 USA

⁵ California Institute of Technology, Division of Geological and Planetary Sciences, MS 150-21, Pasadena, CA 91125, USA

⁶ Centre d'étude Spatiale des Rayonnements, Université de Toulouse [UPS], 31062 Toulouse Cedex 9, France

⁷ CNRS/INSU, UMR 5187, 9 avenue du Colonel Roche, 31028 Toulouse Cedex 4, France

⁸ Laboratoire d'Astrophysique de l'Observatoire de Grenoble, BP 53, 38041 Grenoble, Cedex 9, France.

⁹ Centro de Astrobiología (CSIC/INTA), Laboratorio de Astrofísica Molecular, Ctra. de Torrejón a Ajalvir, km 4 28850,

Torrejón de Ardoz, Madrid, Spain

¹⁰ LERMA, CNRS UMR8112, Observatoire de Paris and École Normale Supérieure, 24 Rue Lhomond, 75231 Paris Cedex 05, France

¹¹ LPMAA, UMR7092, Université Pierre et Marie Curie, Paris, France

¹² LUTH, UMR8102, Observatoire de Paris, Meudon, France

¹³ Jet Propulsion Laboratory, Caltech, Pasadena, CA 91109, USA

¹⁴ Departments of Physics, Astronomy and Chemistry, Ohio State University, Columbus, OH 43210, USA

¹⁵ National Research Council Canada, Herzberg Institute of Astrophysics, 5071 West Saanich Road, Victoria, BC V9E 2E7, Canada

¹⁶ Infrared Processing and Analysis Center, California Institute of Technology, MS 100-22, Pasadena, CA 91125

¹⁷ Canadian Institute for Theoretical Astrophysics, University of Toronto, 60 St George St, Toronto, ON M5S 3H8, Canada

¹⁸ Harvard-Smithsonian Center for Astrophysics, 60 Garden Street, Cambridge MA 02138, USA

¹⁹ National University of Ireland Maynooth, Ireland

²⁰ Department of Physics and Astronomy, Johns Hopkins University, 3400 North Charles Street, Baltimore, MD 21218, USA

²¹ SRON Netherlands Institute for Space Research, PO Box 800, 9700 AV, Groningen, The Netherlands

²² Department of Physics and Astronomy, University of Calgary, 2500 University Drive NW, Calgary, AB T2N 1N4, Canada

²³ University of Massachusetts, Astronomy Dept., 710 N. Pleasant St., LGRT-619E, Amherst, MA 01003-9305 U.S.A

²⁴ LERMA & UMR8112 du CNRS, Observatoire de Paris, 61, Av. de l'Observatoire, 75014 Paris, France

Acknowledgements. HIFI has been designed and built by a consortium of institutes and university departments from across Europe, Canada and the United States under the leadership of SRON Netherlands Institute for Space Research, Groningen, The Netherlands and with major contributions from Germany, France and the US. Consortium members are: Canada: CSA, U.Waterloo; France: CESR, LAB, LERMA, IRAM; Germany: KOSMA, MPIfR, MPS; Ireland, NUI Maynooth; Italy: ASI, IFSI-INAF, Osservatorio Astrofisico di Arcetri- INAF; Netherlands: SRON, TUD; Poland: CAMK, CBK; Spain: Observatorio Astronómico Nacional (IGN), Centro de Astrobiología (CSIC-INTA). Sweden: Chalmers University of Technology - MC2, RSS & GARD; Onsala Space Observatory; Swedish National Space Board, Stockholm University - Stockholm Observatory; Switzerland: ETH Zurich, FHNW; USA: Caltech, JPL, NHSC. Support for this work was provided by NASA through an award issued by JPL/Caltech. CSO is supported by the NSF, award AST-0540882.

H.S.P.M. is very grateful to the Bundesministerium für Bildung und Forschung (BMBF) for financial support aimed at maintaining the Cologne Database for Molecular Spectroscopy, CDMS. This support has been administered by the Deutsches Zentrum für Luft- und Raumfahrt (DLR). We appreciate funding for the ASTRONET Project CATS through the Bundesministerium für Bildung und Forschung (BMBF).

We thank an anonymous referee for constructive comments which helped to clarify the discussion in this article.

Table A.1. Quantum numbers of rotational transitions of H_2O^+ described in the present work, calculated frequencies (MHz) with uncertainties in parentheses^a; lower state energies E_{l_0} (K) and Einstein A -values (10^{-3} s^{-1})

$N''_{K'_a K'_c} - N''_{K''_a K''_c}$	$J' - J''$	$F' - F''$	frequency	E_{l_0}	A
<i>1₁₀ - 1₀₁, para</i>					
1.5 - 0.5	<i>b</i>		604678.6 (25)	0.005	1.3
1.5 - 1.5	<i>b</i>		607227.3 (19)	0.000	6.2
0.5 - 0.5	<i>b</i>		631724.1 (37)	0.005	5.6
0.5 - 1.5	<i>b</i>		634272.9 (24)	0.000	2.8
<i>1₁₁ - 0₀₀, ortho</i>					
1.5 - 0.5	1.5 - 0.5		1115150.75 (85)	0.122	17.1
1.5 - 0.5	0.5 - 0.5		1115186.18 (81)	0.122	27.5
1.5 - 0.5	2.5 - 1.5		1115204.15 (82)	0.000	31.0
1.5 - 0.5	1.5 - 1.5		1115262.90 (82)	0.000	13.9
1.5 - 0.5	0.5 - 1.5		1115298.33 (87)	0.000	3.5
0.5 - 0.5	0.5 - 0.5		1139541.54 (103)	0.122	3.7
0.5 - 0.5	1.5 - 0.5		1139560.58 (94)	0.122	14.8
0.5 - 0.5	0.5 - 1.5		1139653.69 (94)	0.000	29.4
0.5 - 0.5	1.5 - 1.5		1139672.73 (103)	0.000	18.3

^a Numbers in parentheses are 1σ uncertainties in units of the least significant figures. These values should be viewed with some caution, in particular for the *para* transition, see text.

^b F is redundant for *para* transitions; $F = J$ may be assumed. The lowest *para* state is 30.01 K above the lowest *ortho* state.

Appendix A: The spectroscopy of H_2O^+

The rotational spectrum of oxidaniumyl was measured by laser magnetic resonance (LMR) (Strahan et al., 1986; Mürtz et al., 1998); further infrared and electronic spectral measurements have been summarized in Zheng et al. (2008). Observations of the $N_{K_a K_c} = 1_{11} - 0_{00}$, $J = 1.5 - 0.5$ fine structure component near 1115 GHz with *Herschel*/HIFI (Ossenkopf et al., 2010) as well as subsequent observations raised the issue which of the two sets of spectroscopic parameters from LMR measurements provide more reliable frequency predictions. Latest observations as well as reinterpretations of older ones favor the parameters from Mürtz et al. (1998) even though there seem to be small discrepancies of order of ± 5 MHz or 1.35 km s^{-1} between various observations for the specific transition mentioned above. Observations carried out toward Sgr B2(M) or Orion KL for the HEXOS program are probably less suited to derive rest frequencies than certain other observations. Therefore, a preliminary catalog entry has been constructed for the CDMS catalog (Müller et al., 2001, 2005); the final entry is intended to be a common CDMS and JPL (Pickett et al., 1998) catalog entry.

All infrared data and all ground state combination differences (GSCDs) derived from electronic spectra as summarized in Zheng et al. (2008) were used in the fit as long as they were deemed reliable. These data are uncertain to between 0.005 and 0.030 cm^{-1} or between 150 and 900 MHz. Mürtz et al. (1998) provided for their measured data extrapolated zero-field frequencies as well as residuals between observed and calculated frequencies along with uncertainties. From these data weighted averages of the hypothetical experimental zero-field frequencies and of their uncertainties were derived; these uncertainties were of order of 2 MHz with a considerable scatter. Strahan et al. (1986) do not give sufficient data for this purpose. However, Mürtz et al. (1998) published calculated frequencies for the $1_{11} - 0_{00}$ transition. Because of the importance of this transition for

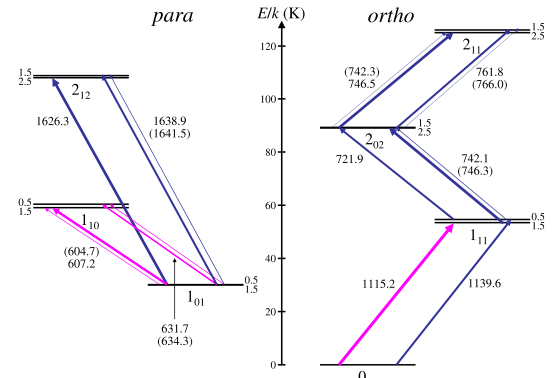


Fig. A.1. Detail of the energy level diagram of H_2O^+ . Hyperfine splitting has been omitted for the *ortho*-levels. Rotational level assignments $N_{K_a K_c}$ are given below the levels, fine structure level assignments J to the side. Magenta arrows mark transitions observed in the course of the present investigation. All other transitions shown can be observed with HIFI. The thickness of the arrows indicates the relative strengths of the transitions and the numbers the approximate frequencies. Frequencies of the weaker components are given in parentheses. The only transitions connecting to levels with $N = 1$ which are not shown are $2_{21} - 1_{10}$ and $2_{20} - 1_{11}$ near 2.85 and 3.0 THz which are not observable with HIFI but with PACS.

the astronomical observation as well as for the fit, these calculated frequencies were also used in the fit with presumable uncertainties corresponding to 2 MHz. The quantum numbers, calculated frequencies, and uncertainties for the two observed rotational transitions are given in Table A.1. Even though the LMR data fit well within their uncertainties, the calculated frequencies should be viewed with some caution because it is not clear how reliable the zero-field extrapolation is. Moreover, the large centrifugal distortion effects affecting the spectra of this ion require additional caution with respect to any extrapolation. It is worthwhile mentioning that the $1_{11} - 0_{00}$ transition frequencies in that table are essentially identical to the ones given in Mürtz et al. (1998). The situation is different for the $1_{10} - 1_{01}$ transition. The $J = 1.5 - 1.5$ fine structure splitting derived from term values given in Table V of Mürtz et al. (1998) differs from the value in Table A.1 by less than 4 MHz whereas the remaining fine structure intervals differ by up to 80 MHz. On the other hand, calculations directly from the Mürtz et al. (1998) parameters differ from values in Table A.1 by less than 10 MHz. As can be seen in Fig. A.1, the ground state *para* level 1_{01} of H_2O^+ is ~ 30.13 and 30.01 K above the 0_{00} level for the $J = 0.5$ and 1.5 fine structure components respectively. Both *para* and *ortho* ground state levels are split into 2 because of the fine and hyper fine structure splitting, respectively. The quantum numbers are 0.5 and 1.5 in both cases, giving $g = 2$ and 4, respectively, and hence $Q \approx 6$ at low temperatures if *ortho* and *para* states are treated independently. This 1 : 1 ratio for Q at low temperatures approaches 3 : 1 at room temperature; it is about 1.5 : 1 and 2 : 1 at ~ 40 and 75 K, respectively. Table A.2 gives selected partition function values for *para*- and *ortho*- H_2O^+ , assuming they are completely non-interacting species.

The mixing of *ortho* and *para* states can be mediated by terms such the off-diagonal electron spin-hydrogen nuclear spin coupling term T_{ab} or the off-diagonal hydrogen nuclear spin coupling term $C_{ab} + C_{ba}$. The radical NH_2 and PH_2 are isoelec-

Table A.2.

T	$Q(para)$	$Q(ortho)$
300.0	109.1787	296.3567
225.0	73.4887	192.9372
150.0	43.0579	105.7512
75.0	19.0770	38.3647
37.5	10.4751	14.5910
18.750	7.3879	7.3124
9.375	6.2329	6.0584
5.000	5.9680	5.9982
2.725	5.9123	5.9961

tronic and isovalent to H_2O^+ . Model calculations have shown the largest perturbations to occur between the 1_{01} and 1_{11} levels, but they are with less than 5 (Gendriesch et al., 2001) and less than 3 kHz (Margulès et al., 2002), respectively, rather small, maybe even negligible. Model calculations suggest that perturbations of the two rotational transitions described in the present study are less than 3 kHz. Slightly larger perturbations may occur at higher quantum numbers.